1

2 **Seeing is believing: methods to monitor vertebrate autophagy *in vivo***

3

4 Ana Lopez Ramirez[1,2], Angeleen Fleming[1,2] and David C. Rubinsztein[1,3*]

5

6 [1]Department of Medical Genetics, University of Cambridge, Cambridge Institute for Medical

7 Research, Wellcome Trust/MRC Building, Cambridge Biomedical Campus, Hills Road,

8 Cambridge, CB2 0XY. United Kingdom.

9 [2]Department of Physiology, Development and Neuroscience, University of Cambridge,

10 Downing Street, Cambridge CB2 3DY, UK.

11 [3] UK Dementia Research Institute, University of Cambridge, Cambridge Institute for Medical

12 Research, Wellcome Trust/MRC Building, Cambridge Biomedical Campus, Hills Road,

13 Cambridge, CB2 0XY. United Kingdom.

14

15 *Corresponding author: dcr1000@cam.ac.uk

16

17

18

Autophagy is an intracellular clearance pathway that delivers cytoplasmic contents to the lysosome for degradation. It plays a critical role in maintaining protein homeostasis and providing nutrients under conditions where the cell is starved. It also helps to remove damaged organelles and misfolded or aggregated proteins. Thus, it is not surprising that defects in this pathway are associated with a variety of pathological conditions, such as neurodegeneration, cancer and infection. Pharmacological upregulation of autophagy is considered a promising therapeutic strategy for the treatment of neurodegenerative and infectious diseases. Studies in knockout mice have demonstrated that autophagy is essential for nervous system function and data from invertebrate and vertebrate models suggest that the efficiency of autophagic processes generally declines with age. However, much of our understanding of the intracellular regulation of autophagy comes from *in vitro* studies and there is a paucity of knowledge about how this process is regulated within different tissues and during the processes of aging and disease. Here, we review the available tools to probe these questions *in vivo* within vertebrate model systems. We discuss how these tools have been used to date and consider future avenues of research.

35

Autophagy cell biology

In the initial steps of autophagy, a double-membraned cup-shaped precursor (called the phagophore) forms within the cytoplasm. The phagophore expands, engulfing substrates as it does so and eventually the edges fuse to form a double-membraned vesicle, the autophagosome. This traffics along microtubules to the lysosome, with which it fuses resulting in the degradation of the autophagic contents (Fig. 1). Autophagy is controlled through a conserved family of approximately thirty core genes that encode the autophagic machinery, termed the AuTophaGy-related (*atg*) gene family (Feng et al., 2014). The *atg* genes were originally discovered in yeast; mutations in these genes resulted in an inability to survive

45   nutrient deprivation conditions. Most of these genes have vertebrate homologs that are named

46   after their yeast counterparts. Interestingly, many of the yeast genes have more than one

47   vertebrate homolog (Feng et al., 2014; Mizushima et al., 2011), which may contribute to either

48   redundancy or to additional functional diversity.

49

50   To follow this process *in vivo*, it is necessary to label and visualise the phagophores and

51   autophagosomes. However, few proteins are uniquely associated with autophagic vesicles

52   and their precursors, with only one protein (LC3-II) known to label autophagic structures both

53   prior to and after fusion with the lysosome. LC3 is one of several vertebrate homologues of

54   ATG8. Mammalian cells have six ATG8 orthologues; the MAP1-LC3 (LC3) and GABARAP

55   subfamilies (microtubule-associated protein 1 light chain 3 and GABA(A) receptor-associated

56   protein families respectively), while zebrafish have eight (see Table 1). During

57   autophagosome formation, these ATG8-family proteins are conjugated to the lipid

58   phosphatidylethanolamine (PE) in autophagosomal membranes. This lipidation requires a

59   protease and two ubiquitin-like conjugation systems (Ichimura et al., 2000; Mizushima et al.,

60   1998)(Fig 1). ATG4 is a cysteine protease that cleaves the C-terminus of LC3 exposing a

61   glycine residue. This first cleaved form of LC3 is called LC3-I. A further reaction then occurs

62   involving a complex of ATG proteins that act as an E3-like ligase. This determines the site of

63   LC3 lipidation and assists the transfer of LC3-I to PE to form LC3-II (Ichimura et al., 2000).

64

65   Since lipidated ATG8 proteins (such as LC3-II) are the only proteins which associate with pre-

66   autophagosomal structures, autophagosomes and autolysosomes, they are widely accepted

67   as being the best marker to distinguish autophagic vesicles from other cellular membranes

68   (Klionsky et al., 2016; Mizushima et al., 2010). Measuring LC3 lipidation by western blotting,

69   counting the number of LC3 vesicles by immunofluorescence or with fluorescently tagged LC3

70   expression constructs, and detecting the degradation of long-lived proteins or damaged

71   organelles are the most commonly used methods for monitoring autophagy (Klionsky et al.,

72   2016; Mizushima et al., 2010). However, care must be taken in interpreting increases in LC3

73 levels as this may occur as a result of an increase in autophagosome formation (upregulation)

74 or a blockage in clearance. In the latter scenario, autophagosomes are not degraded typically

75 due to failure to fuse with lysosomes or due to an increase in lysosomal pH, which thereby

76 inactivates the degradative enzymes (see Fig 2).

77

78 The majority of studies using these biochemical or fluorescent detection methods have only

79 provided a snapshot of autophagic activity within a single tissue at a single time. Many studies

80 have reported that basal levels of autophagy differ between different tissues, and we do not

81 fully understand how these different rates are affected by pharmacological upregulation or

82 disease pathology.   Since upregulation of autophagy is considered to be a promising

83 therapeutic strategy for the treatment of a range of disorders including neurodegeneration,

84 infectious disease and cancer (Galluzzi et al., 2015; Rubinsztein et al., 2015), it is vital that we

85 understand how potential therapies act in different tissues and this can only be done by *in vivo*

86 analysis. Similarly, to understand the role of autophagy in the pathogenesis of disease, it is

87 important to study this process in the whole animal to investigate tissue-specific changes in

88 flux, the difference in flux between young and old animals and cell autonomous versus non-

89 cell autonomous effects. In recent years, various transgenic reporters have been developed

90 which may be useful to improve our understanding of autophagy *in vivo*. Together with

91 advances in imaging such as CLEM (correlated light and electron microscopy) and lightsheet

92 microscopy, we now have the tools to interrogate this process in living vertebrate animals.

93 Although such imaging is in its infancy, here we review the available tools and highlight the

94 future possibilities for studying autophagy *in vivo*.

95

96 **Single fluorophore probes**

97 The use of a fusion construct comprising green fluorescent protein (GFP) tagged to LC3 was

98 the first approach to examine autophagy *in vivo* in vertebrates and provided novel insights

99 about its regulation in both physiological and pathological conditions. The overexpression of

100 Atg8 homologs fused with GFP had been previously described in other species, such as yeast,

101 *Caenorhabditis elegans, Dictyostelium discoideum, Drosophila melanogaster* and *Arabidopsis*

102 *thaliana* (Melendez et al., 2003; Otto et al., 2003; Rusten et al., 2004; Yoshimoto et al., 2004).

103 GFP-LC3, like endogenous LC3, becomes conjugated to the phagophore and remains on the

104 membrane after the complete closure of the autophagosome. Autophagosomes labelled with

105 GFP-LC3 are evident as puncta or ring-like structures by fluorescence microscopy (Kabeya et

106 al., 2000; Mizushima et al., 2003; Mizushima et al., 2001). GFP-LC3 can also be found on the

107 membrane of autolysosomes but to a lesser extent. The fluorescent signal of these

108 autolysosomes is weaker and therefore distinguishable from bright autophagosomes (Kabeya

109 et al., 2000).

110 The generation of transgenic mice expressing GFP-LC3 under the control of a ubiquitous

111 promoter has allowed the post-mortem examination of GFP-LC3 localization by high-

112 resolution microscopy and in almost all tissues (Mizushima et al., 2004). The overexpression

113 of GFP-LC3 in mice permits not only qualitative but quantitative analysis of the

114 autophagosome numbers and does not affect endogenous autophagy, since the endogenous

115 ratio of LC3II/LC3-I is maintained. Post-mortem analysis of tissues from this transgenic mouse

116 have been used to measure autophagosome numbers during development (Kuma et al.,

117 2004), under starvation conditions (Mizushima et al., 2004), or in different disease states such

118 as amyotrophic lateral sclerosis (ALS) (Tian et al., 2011), polycystic kidney disease (Tanaka

119 et al., 2016) and cerebral ischaemia (Tian et al., 2010). In addition, primary cultures from these

120 mice have been used for *ex vivo* real-time observations of GFP-LC3 positive autophagic

121 structures (Mizushima, 2009; Mizushima et al., 2004).

122 An important consideration in the analysis of such reporter lines is to determine whether the

123 fluorescent protein is a faithful reporter of the endogenous protein. Mishuzima and colleagues

124 demonstrated by western blot analysis, that the levels of endogenous LC3 and GFP-LC3

125 protein are organ-dependent rather than uniform. In the brain, the level of expression of GFP-

126 LC3 was comparable to endogenous LC3 whereas in other tissues GFP-LC3 was

127   overexpressed. Importantly, the integration of the GFP‑LC3 transgene, upstream of an open

128   reading frame in a pseudogene in the distal region of chromosome 2, did not cause any

129   phenotypic or genetic abnormalities in homozygous mice (Kuma et al., 2007).

130

131   Zebrafish are potentially a more tractable model to study autophagy *in vivo* since they are

132   amenable to a most forms of fluorescent imaging due to their size and transparency.

133   Furthermore, analysis is not restricted to embryonic stages, as their rapid development permits

134   the analysis of functioning organs in larvae at free-swimming stages. Zebrafish have eight

135   homologs of Atg8 (see Table 1) with high sequence similarity to their mammalian orthologues.

136   He *et al.* generated the first transgenic zebrafish autophagy reporter lines for expressing GFP-

137   LC3 and GFP-Gabarap under the control of the constitutive cytomegalovirus (CMV) promoter

138   (He et al., 2009). Both transgenes showed similar expression patterns; expression being

139   especially high in spinal cord, muscle and lens. Similar to mammalian LC3, zebrafish LC3-I

140   conjugates to phosphatidylethanolamine to generate LC3-II. Initial studies reported that LC3-

141   II was only observed in embryos from 24 hours post-fertilization (h.p.f.) onwards by western

142   blotting (He et al., 2009). However Lee *et al.* detected autophagy at approximately 15 h.p.f.,

143   evidenced by the presence autophagosomes visualized as GFP-LC3 puncta in the CMV:GFP-

144   LC3 transgenic reporter line (Lee et al., 2014). The benefit of this model is not only the ability

145   to perform live imaging, but also to examine multiple tissues within the same animal. Imaging

146   of GFP-LC3 transgenic embryos by confocal fluorescence microscopy showed that the GFP-

147   LC3 protein forms few puncta in basal conditions but the number of puncta increase after

148   autophagy upregulation by addition of rapamycin or calpain inhibitors to the embryo medium

149   (He et al., 2009). The fusion of autophagosomes to the lysosomes can also be detected *in*

150   *vivo* by adding Lysotracker to the embryo medium (He et al., 2009). A dramatic increase in

151   the co-localization of LysoTracker red-labelled lysosomes with GFP-LC3 puncta was observed

152   upon the treatment with lysosomal protease inhibitors like pepstatin A or E64d, suggesting

153 that basal autophagic flux is high in these embryonic and early larval stages (2 and 3 d.p.f)

154 (Mathai et al., 2017).

155 Several studies have exploited the ability to perform *in vivo* imaging in this GFP-LC3 zebrafish

156 line, for example to study the role of autophagy in blastema formation and regeneration

157 following fin amputation (Varga et al., 2014), or in the liver to examine autophagic responses

158 to pharmacological manipulation (Cui et al., 2012). The ability to perform transient gene

159 knockdown using morpholino oligonucleotides (Bedell et al., 2011) in zebrafish has enabled

160 the rapid analysis of candidate genes in the regulation of different stages of the autophagy

161 pathway. For example, transient silencing of *Hs1bp3*, a phosphoinositide-binding PX domain

162 containing protein, increased the number of GFP-LC3 puncta visualized directly along the

163 trunk of morphants compared to control embryos and this increase was greater after

164 chloroquine treatment, suggesting increased autophagic flux *in vivo* (Holland et al., 2016). A

165 similar approach was taken to study *spns1*, a putative lysosomal H^+-carbohydrate transporter

166 involved in senescence and in the late stages of the autophagy/lysosome pathway. Morpholino

167 knockdown of *spns1* resulted in an accumulation of GFP puncta visualised by confocal

168 microscopy in live embryos and was also observed in *spns1* mutants (Sasaki et al., 2014).

169 Careful characterisation using lysotracker and mCherry-LC3 transgenic fish demonstrated this

170 was due to a block in autophagosome degradation rather than an increase in autophagosome

171 formation. A dual GFP-LC3;mCherry-Lamp1 reporter line recently developed by the same

172 group was used to further elucidate the role of lysosome acidification in senescence (Sasaki

173 et al., 2017). Although analysis was performed *in vivo* in in these examples, these studies

174 relied on analysis of single timepoint images to assess autophagosome number and did not

175 exploit the full potential of studying these events in the living organism.

176 One example of the power of using zebrafish for *in vivo* observations has been in the study of

177 the innate immune response (Varga et al., 2014). Transgenic reporters have been used to

178 track individual immune cells throughout the whole organism in response to tissue injury or

179 infection and to study features of swarming and resolution of inflammation (Renshaw and

180   Trede, 2012). The combination of *in vivo* light microscopy and *ex vivo* electron microscopy

181   imaging opens new directions for studying the role of autophagy in infectious diseases.

182   Transgenic GFP-LC3 zebrafish infected with *Shigella* have been used to investigate to study

183   the process of bacterial clearance *in vivo.* Engulfed bacteria were observed to be sequestered

184   in GFP-positive autophagosomes (Mostowy et al., 2013), a finding confirmed by post-mortem

185   transmission   electron   microscopy   analysis.   Similarly,   during   *Mycobacterium*

186   *marinum* infection in zebrafish, the bacteria were frequently found associated with GFP-LC3-

187   positive vesicles, and these associations were particularly abundant in leukocytes. By

188   correlative light and electron microscopy, the precise location of intracellular bacteria could be

189   elucidated (either free, in autophagosomes or associated to lysosomes) by determining the

190   ultrastructure of GFP-LC3-positive structures (Hosseini et al., 2014).

191   These studies highlight the importance of verifying the properties of the LC3-labelled

192   structures. Although LC3 is the best-established marker to identify autophagosomes, it can

193   also be associated with single membranes on phagosomes within macrophages and other

194   phagocytic cell types where it functions in a process called LC3-associated phagocytosis

195   (LAP) (Sanjuan et al., 2009). In this instance, following receptor-mediated phagocytosis, LC3

196   is recruited to the single-membrane phagosomes using the same conjugation machinery as is

197   involved with macroautophagy. Therefore, within immune cells, careful interpretation of LC3

198   puncta is required as it may not only detect autophagosomes, but also LC3-labelled

199   phagosomes and correlative light and electron microscopy may be critical in differentiating

200   these processes.

201   Although these transgenic reporters are powerful tools for studying autophagic processes *in*

202   *vivo* or in primary cultures, there are important caveats to consider. GFP-LC3 was initially

203   described to localize exclusively on autophagic membranes. However GFP-LC3 protein can

204   aggregate   in   an   autophagy-independent   manner   without   being   conjugated   to

205   phosphatidylethanolamine leading to misinterpretation of the results, especially during

206   transient expression of the transgene (Kuma et al., 2007). For example, GFP-LC3 can be

207 seen to localise with intracellular protein aggregates like huntingtin inclusions in autophagy-

208 null cell lines suggesting that GFP-LC3 puncta do not always represent autophagic structures

209 and therefore LC3 fluorescent localization should be carefully interpreted. Tanida and

210 colleagues proposed the use of mutant fluorescent LC3 (the human mutation LC3DG) which

211 cannot be lipidated as negative control (Tanida et al., 2008) and as described below,

212 transgenic reporters using this control have now been developed (Kaizuka et al., 2016).

213 Since fluorescently tagged-LC3 labels the surface of all autophagic structures, from the

214 formation of the phagophore to the autolysosome, no conclusions can be made about

215 autophagy flux or dynamics by simply measuring the number of puncta. An increase in GFP-

216 LC3 puncta may occur as a result of an increase autophagosome formation but also could be

217 the consequence of an impairment of autolysosome formation (Klionsky et al., 2016). In cell

218 culture, the inhibition of vacuolar acidification and consequent inhibition of lysosomal activity

219 by bafilomycin A1 (Baf) treatment is commonly employed as a tool to investigate changes in

220 autophagic flux (Rubinsztein et al., 2009). Such treatment prevents the downstream clearance

221 of autophagosomes and allows a comparison of number of puncta in the presence or absence

222 of lysosomal degradation (Klionsky et al., 2016). *In vivo*, chloroquine or ammonium chloride

223 treatments may be employed to reduce vacuolar acidification, although these treatments are

224 likely to be toxic at saturating concentrations and therefore, at best, can only be considered to

225 be a partial lysosomal block. Such an approach has been used to measure cardiac autophagic

226 flux *in vivo* in mCherry-LC3 transgenic mice (Iwai-Kanai et al., 2008). A clearer differentiation

227 between GFP-LC3 associated with autophagosomes or with acidic lysosomes can be

228 achieved by labelling acidic structures with LysoTracker (He et al., 2009; Sasaki et al., 2014)

229 or with the use of additional transgenic lysosome markers such as mCherry-Lamp1 (Sasaki et

230 al., 2017). If the co-localization of acidic structures with fluorescent LC3 puncta increases with

231 respect to the total number of labelled structures, this may be indicative of an induction in

232 autophagy. However, this may also occur if there is defective lysosomal function causing

233   delayed LC3 degradation, for example as observed when components of the chaperonin

234   complex are depleted (Pavel et al., 2016).

235   A further important consideration is the degradation of GFP-LC3, which can generate free

236   GFP fragments that may accumulate depending on the acidity of the lysosomes and

237   degradative capacity of lysosomal compartments (Ni et al., 2011). In cell culture, LC3 was

238   found to be degraded faster than GFP from GFP-LC3 since GFP degradation requires high

239   lysosomal acidification. Starvation, rapamycin or incomplete suppression of autophagy by low

240   doses of inhibitors of lysosomal acidification such as chloroquine (CQ) or Baf also led to higher

241   levels of free GFP fragments from GFP-LC3 in several mammalian cell lines expressing GFP-

242   LC3 (Hosokawa et al., 2006) and similarly in the liver of GFP-LC3 transgenic mice following

243   CQ treatment (Ni et al., 2011). However, it is important to note that this phenomenon and its

244   utility varies in different mammalian cell types and cell lines and this method has not been

245   widely used in mammalian systems.

246

247   **Dual fluorophore probes**

248   Since the GFP fluorescent signal is quenched in the acidic environment of autolysosomes,

249   this limits the utility of this reporter for tracking vesicles during the autophagic process. To

250   overcome these limitations, a tandem fluorescent tagged-LC3 was developed and initially

251   characterised *in vitro* (Kimura et al., 2007). The fluorescent proteins GFP and mRFP have

252   different properties under acidic conditions. Kimura and collaborators showed that using a

253   tandem-tagged mRFP-GFP-LC3, GFP fluorescence (pKa 5.9) is quenched in the acidic

254   environment of the lysosomes, whereas the red fluorescence from the mRFP tag (pKa 4.5) is

255   maintained due to its different sensitivity to pH. As a consequence, GFP channels and mRFP

256   channels of the same labelled cells showed different distribution patterns of puncta. The

257   development of the tandem fluorescent mRFP-GFP-LC3 has been widely used *in vitro* to study

258   the mechanisms regulating the maturation of autophagosomes and the fusion to lysosomes

259 in the degradative process. Due to this pH-dependent quenching of the GFP-LC3

260 fluorescence, only mRFP-LC3 can be detected in autolysosomes (i.e. these appear red only),

261 whereas autophagosomes can be visualised by both fluorophores (i.e. these appear orange)

262 (see Fig.3).

263 The first *in vivo* mouse model expressing mRFP-GFP-LC3 was generated by Li and

264 colleagues in 2014 (Li et al., 2014). Expression of the LC3 tandem reporter was ubiquitous,

265 which allowed a better understanding of the dynamics of autophagy *in vivo* under stress

266 conditions, such as starvation and disease. In these RFP-EGFP-LC3 mice, autophagic

267 vacuoles were visualised as RFP- and EGFP-positive puncta, similar to *in vitro* observations

268 in cells expressing the same construct. The model was first used to evaluate the role of

269 autophagy in ischemia-reperfusion injury in the kidney using primary cell culture. In addition,

270 primary cortical neurons from an independently generated mouse line have been used to

271 investigate the interplay between chaperone proteins and autophagy (Pavel et al., 2016).

272 Tandem construct mCherry- or RFP-GFP-LC3 have also been used in zebrafish. Transient

273 expression of RFP-GFP-LC3 in zebrafish was used to investigate the autophagy pathway in

274 the clearance of mycobacterium infection. Treatment with carbamazepine was shown to

275 improve the clearance of mycobacterial infection *in vivo* and increase autophagic flux in larvae

276 zebrafish (Schiebler et al., 2015). Stable transgenic zebrafish expressing mCherry-GFP-

277 map1lc3b have also been used to evaluate the autophagic and late endosomal trafficking

278 pathways in the cone photoreceptors of *synJ1*-deficient zebrafish (Allwardt et al., 2001;

279 George et al., 2016; Van Epps et al., 2001). Live time-lapse confocal microscopy revealed an

280 increase in the formation of autophagosome precursors and a defect in autophagosome

281 maturation *in vivo* in *synJ1*-deficient zebrafish, resulting in the accumulation of

282 autophagosomes. Modulation of the PI(4,5)P2 regulator, Arf6, by expressing a constitutively

283 active mutant of Arf6, rescued the defects seen in cones of synJ1-deficient fish. These results

284 suggest that Arf6a modulates positively the levels of PI(4,5)P2, substrate for SynJ1, and hence

285 that both Arf6 and SynJ1 play a role in the same pathway to regulate autophagy in cone

286 photoreceptors (George et al., 2016). These studies highlight the potential of the zebrafish
287 model to characterize aspects of vesicle transport *in vivo*.

288 However, as with the analysis of GFP-tagged LC3, there are additional factors to be
289 considered when using this tandem red-green fluorescent LC3 fusion protein. Firstly, the red
290 and green fluorescence from unconjugated LC3 exists in the cytosol of all cells. When
291 autophagic flux is low, this background is higher. As the LC3 becomes conjugated and more
292 puncta appear, the background fluorescence decreases (see Fig. 3). Identifying puncta
293 against this fluorescent background is challenging and care must be taken in quantifying the
294 number of autophagosomes in conditions where the background fluorescence changes.
295 Secondly, due to the pH-sensitivity of the GFP signal, reduction in the green signal may
296 depend not only on the enzymatic degradation of GFP itself but also the speed at which the
297 lysosomal content acidifies (Mizushima et al., 2010). Thus, what one is formally assessing are
298 the numbers of unacidified versus acidified LC3-containing vesicles, which may not always be
299 the same as the numbers of autophagosomes prior to lysosome fusion versus autolysosomes.

300 The development of new generation of fluorescent probes may help with some of these
301 difficulties. A new dual fluorescence probe was recently generated by the Mizushima group
302 comprising GFP-LC3-RFP-LC3DG (Kaizuka et al., 2016). The expression of the construct
303 results a protein that is cleaved by Atg4 proteases resulting in the equimolar amounts of two
304 separate fluorescently tagged proteins; GFP-LC3 and RFP-LC3DG. RFP-LC3DG is a mutated
305 form of LC3, which cannot be conjugated (see Fig. 4). It is therefore unable to attach to
306 autophagic membranes, remaining in the cytosol and hence can be used as an internal
307 control. However, GFP-LC3 can be lipidated and attaches to the autophagosome membrane.
308 GFP-LC3 on the inner autophagosome membrane is degraded by autophagy whereas on the
309 outer membrane it is deconjugated by Atg4 and returns to the cytosol. The ratio of GFP/RFP
310 can therefore be used as a measurement of autophagic flux as it assesses LC3 degradation
311 via a conjugation-dependent route (i.e. autophagy). However, as only a small proportion of the
312 protein is degraded the windows of detection are limited.

313 Mice and zebrafish expressing GFP-LC3-RFPLC3DG were developed to evaluate autophagic

314 flux in different tissues and validated to confirm that the reporter responds appropriately to

315 drug induced autophagy upregulation (Kaizuka et al., 2016). Although the transgene was

316 detected in several tissues by western blotting in mice, only skeletal muscle showed sufficient

317 levels of expression for fluorescence analysis. Post-mortem analysis of muscle sections was

318 used to evaluate fed versus fasted conditions. Interestingly, their findings suggest that slow

319 and fast twitch muscle fibres have different levels of basal autophagy (Kaizuka et al., 2016).

320 The use of other fluorescent tandem reporters with different pH-sensitivities, such as mWasabi

321 (pKa at 6.5 vs. pKa 5.9 of GFP) leads to a faster loss of fluorescence in the autolysosomes

322 (Zhou et al., 2012) and may be a better tool for tracking autophagy flux *in vivo*. Both mTagRFP

323 and mWasabi-LC3 are much brighter than mRFP/mCherry and EGFP fluorescence. mWasabi

324 is also more acid-sensitive than EGFP and hence more easily quenched in the acidic

325 environment of autolysosomes (Chudakov et al., 2010). In addition, the pKa of mTagRFP (4.0)

326 is lower than that of mRFP (4.5) suggesting that mTagRFP is more stable than mRFP in acidic

327 conditions (Shaner et al., 2004). These characteristics make discrimination of autolysosomes

328 and autophagosomes more accurate than other fluorophores and were used to investigate the

329 dose-dependent effect of autophagy inducers in the autophagic flux in cells (Zhou et al., 2012).

330 However, no *in vivo* models have been created using this construct. Similarly Rosella, a

331 tandem reporter of the fast maturing red fluorescent protein dsRed.T3 with GFP, has been

332 used being successfully used to track labelled cytosolic proteins, mitochondria or the nucleus

333 to the autophagic vacuole in yeast (Mijaljica et al., 2011; Rosado et al., 2008). Rosella-LC3

334 and Mito-Rosella biosensors have been developed and characterised in HeLa cells (Sargsyan

335 et al., 2015). These authors reported that transgenic mouse models for Rosella-LC3 and Mito-

336 Rosella biosensors were being developed to measure mitophagy and autophagic flux in

337 different tissues *in vivo*, although no further data have been published to date.

338

339 **pH-sensitive probes**

340   In contrast to the use of dual fluorophores to label LC3, new approaches have been developed

341   in recent years which allow one to measure autophagic flux using a single fluorophore.

342   dKeima, a coral-derived fluorophore, has a bimodal excitation spectrum (438 and 550 nm)

343   with an emission spectrum peak at 620 nm (Kogure et al., 2006). The different excitation

344   wavelengths correspond to the neutral and ionized states of the chromophore with the neutral

345   state (438 nm excitation) predominant at neutral/high pH and the ionized state (550 nm

346   excitation) more abundant at low pH. Therefore dual excitation ratiometric imaging (438/550

347   nm) can be used to determine the environmental pH (Katayama et al., 2011). In cell culture

348   experiments, dKeima was demonstrated to be delivered to lysosomes via the autophagic

349   pathway and was observed to accumulate inside the lysosomal compartments because it is

350   resistant to degradation by lysosomal proteases (Katayama et al., 2011). Hence ratiometric

351   imaging over time can be used to monitor the maturation of autolysosomes and therefore

352   autophagic flux. Furthermore, since the emission spectrum of dKeima peaks at 620 nm, this

353   probe can be simultaneously imaged with green fluorophores (e.g. EGFP-LC3) without cross-

354   detection or excitation (Katayama et al., 2011).

355   In addition, Keima can be targeted to either proteins or organelles. For example, Keima

356   targeted to mitochondria (Mito-Keima) has been used to evaluate mitochondrial autophagy

357   (mitophagy) in cell culture (Katayama et al., 2011). Mito-Keima has also been used in mice

358   via intravenous injection of adeno-associated virus (AVV9) harbouring either Mito-Keima or

359   Lamp1-YFP (yellow fluorescent protein) to evaluate mitophagy in cardiomyocytes of the adult

360   heart (Shirakabe et al., 2016). Confocal imaging of thin slices of the heart showed Lamp1-

361   YFP dots colocalizing with acidic Mito-Keima (561 nm) after 48-hour starvation of the animals,

362   suggesting that the lysosomal degradation of mitochondria is stimulated after fasting.

363   **Labelling autophagic substrates**

364   An alternative approach is not to measure autophagosomes *per se* but to measure the

365   clearance of autophagic substrates. Tau is a microtubule associated protein which is known

366   to be an autophagy substrate (Lee et al., 2013). Zebrafish models have been developed

367 expressing a transgenic construct comprising human tau tagged with the photoconvertible

368 fluorescent protein, Dendra. The fluorescently tagged tau protein is visible as green

369 fluorescence but this can be converted to a red fluorescent protein by exposure to 405 nm

370 wavelength light. This conversion labels a steady-state pool of tau protein allowing clearance

371 kinetics to be measured without being confounded by new protein synthesis (since newly

372 formed protein will be green). This method has been used to assess both genetic modifiers

373 of tau clearance (Moreau et al., 2014) and also to assess clearance of wildtype and mutant

374 forms of tau in response to autophagy stimulus (Lopez et al., 2017). Such studies have

375 provided the first observations of substrate clearance in neurons *in vivo* (see Fig. 5). This

376 approach has also been used to study the clearance of mutant huntingtin in cell culture

377 (Tsvetkov et al., 2013). Although clearance of substrates is likely affected by both the

378 proteasome and autophagy, the use of proteasome blocking agents (e.g. MG132) and

379 lysosomal acidification inhibitors (e.g. Baf, CQ or ammonium chloride) allows discrimination

380 between the two clearance pathways and an assessment of the relative contribution of each.

381

382 **Future directions/conclusions**

383 To date, much of our understanding of autophagosome formation, trafficking and degradation

384 have come from work in cell lines or in primary cell culture. The elegant work of the Holzbaur

385 group in studying trafficking in primary neurons has revealed important aspects of

386 autophagosome trafficking and biogenesis (Fu et al., 2014; Maday and Holzbaur, 2014; Maday

387 and Holzbaur, 2016). Given the tools described here, and the advances imaging techniques,

388 it is likely that we now have the ability to investigate many of these processes *in vivo.* Indeed,

389 such approaches have been applied to the *in vivo* trafficking of mitochondria (Drerup et al.,

390 2017; Dukes et al., 2016; Plucinska et al., 2012). Caveats remain about the fidelity of

391 transgenicly labelled proteins, since these protein-tags are expressed in addition to the

392 endogenous protein, typically at higher levels than the endogenous protein and are not

393 controlled by the endogenous promoter. However, chromobody labelling may be one

394 approach that can be used to overcome this. These are small antigen recognising elements

395 (nanobodies) fused to fluorescent reporters and have been used to label actin cytoskeleton

396 and cell cycle associated proteins in zebrafish (Panza et al., 2015). In addition, recent

397 advances in CRISPR- and TALEN- mediated knock-in methodologies (Albadri et al., 2017;

398 Schmid-Burgk et al., 2016) suggest that in future it may be possible to specifically add tags to

399 endogenous proteins. Therefore, although we have not yet exploited the full power of the

400 transgenic, genomic editing and imaging technologies, the tools are now available to allow us

401 to better investigate the process of autophagy in health and disease within living tissues. Since

402 autophagy impacts on a diverse range of pathological conditions such as neurodegeneration,

403 infection and cancer, the ability to visualise how autophagic flux is affected *in vivo* in such

404 disease states will provide valuable information on which steps of the pathway can be

405 manipulated for therapeutic benefit.

406

407

408

409 ACKNOWLEDGEMENTS:

414

415

416

417

References

Albadri, S., Del Bene, F. and Revenu, C. (2017). Genome editing using CRISPR/Cas9-based knock-in approaches in zebrafish. *Methods* **121-122**, 77-85.

Allwardt, B. A., Lall, A. B., Brockerhoff, S. E. and Dowling, J. E. (2001). Synapse formation is arrested in retinal photoreceptors of the zebrafish nrc mutant. *J Neurosci* **21**, 2330-42.

Bedell, V. M., Westcot, S. E. and Ekker, S. C. (2011). Lessons from morpholino-based screening in zebrafish. *Brief Funct Genomics* **10**, 181-8.

Chudakov, D. M., Matz, M. V., Lukyanov, S. and Lukyanov, K. A. (2010). Fluorescent proteins and their applications in imaging living cells and tissues. *Physiol Rev* **90**, 1103-63.

Cui, J., Sim, T. H., Gong, Z. and Shen, H. M. (2012). Generation of transgenic zebrafish with liver-specific expression of EGFP-Lc3: a new in vivo model for investigation of liver autophagy. *Biochem Biophys Res Commun* **422**, 268-73.

Drerup, C. M., Herbert, A. L., Monk, K. R. and Nechiporuk, A. V. (2017). Regulation of mitochondria-dynactin interaction and mitochondrial retrograde transport in axons. *Elife* **6**.

Dukes, A. A., Bai, Q., Van Laar, V. S., Zhou, Y., Ilin, V., David, C. N., Agim, Z. S., Bonkowsky, J. L., Cannon, J. R., Watkins, S. C. et al. (2016). Live imaging of mitochondrial dynamics in CNS dopaminergic neurons in vivo demonstrates early reversal of mitochondrial transport following MPP(+) exposure. *Neurobiol Dis* **95**, 238-49.

Feng, Y., He, D., Yao, Z. and Klionsky, D. J. (2014). The machinery of macroautophagy. *Cell Res* **24**, 24-41.

Fu, M. M., Nirschl, J. J. and Holzbaur, E. L. F. (2014). LC3 binding to the scaffolding protein JIP1 regulates processive dynein-driven transport of autophagosomes. *Dev Cell* **29**, 577-590.

Galluzzi, L., Pietrocola, F., Bravo-San Pedro, J. M., Amaravadi, R. K., Baehrecke, E. H., Cecconi, F., Codogno, P., Debnath, J., Gewirtz, D. A., Karantza, V. et al. (2015). Autophagy in malignant transformation and cancer progression. *EMBO J* **34**, 856-80.

444 **George, A. A., Hayden, S., Stanton, G. R. and Brockerhoff, S. E.** (2016). Arf6 and the
445 5'phosphatase of synaptojanin 1 regulate autophagy in cone photoreceptors. *Bioessays* **38**
446 **Suppl 1**, S119-35.

447 **He, C., Bartholomew, C. R., Zhou, W. and Klionsky, D. J.** (2009). Assaying autophagic
448 activity in transgenic GFP-Lc3 and GFP-Gabarap zebrafish embryos. *Autophagy* **5**, 520-6.

449 **Holland, P., Knaevelsrud, H., Soreng, K., Mathai, B. J., Lystad, A. H., Pankiv, S.,**
450 **Bjorndal, G. T., Schultz, S. W., Lobert, V. H., Chan, R. B. et al.** (2016). HS1BP3 negatively
451 regulates autophagy by modulation of phosphatidic acid levels. *Nat Commun* **7**, 13889.

452 **Hosokawa, N., Hara, Y. and Mizushima, N.** (2006). Generation of cell lines with tetracycline-
453 regulated autophagy and a role for autophagy in controlling cell size. *FEBS Lett* **580**, 2623-9.

454 **Hosseini, R., Lamers, G. E., Hodzic, Z., Meijer, A. H., Schaaf, M. J. and Spaink, H. P.**
455 (2014). Correlative light and electron microscopy imaging of autophagy in a zebrafish infection
456 model. *Autophagy* **10**, 1844-57.

457 **Ichimura, Y., Kirisako, T., Takao, T., Satomi, Y., Shimonishi, Y., Ishihara, N., Mizushima,**
458 **N., Tanida, I., Kominami, E., Ohsumi, M. et al.** (2000). A ubiquitin-like system mediates
459 protein lipidation. *Nature* **408**, 488-92.

460 **Iwai-Kanai, E., Yuan, H., Huang, C., Sayen, M. R., Perry-Garza, C. N., Kim, L. and Gottlieb,**
461 **R. A.** (2008). A method to measure cardiac autophagic flux in vivo. *Autophagy* **4**, 322-9.

462 **Kabeya, Y., Mizushima, N., Ueno, T., Yamamoto, A., Kirisako, T., Noda, T., Kominami,**
463 **E., Ohsumi, Y. and Yoshimori, T.** (2000). LC3, a mammalian homologue of yeast Apg8p, is
464 localized in autophagosome membranes after processing. *EMBO J* **19**, 5720-8.

465 **Kaizuka, T., Morishita, H., Hama, Y., Tsukamoto, S., Matsui, T., Toyota, Y., Kodama, A.,**
466 **Ishihara, T., Mizushima, T. and Mizushima, N.** (2016). An Autophagic Flux Probe that
467 Releases an Internal Control. *Mol Cell* **64**, 835-849.

468 **Katayama, H., Kogure, T., Mizushima, N., Yoshimori, T. and Miyawaki, A.** (2011). A
469 sensitive and quantitative technique for detecting autophagic events based on lysosomal
470 delivery. *Chem Biol* **18**, 1042-52.

471 **Kimura, S., Noda, T. and Yoshimori, T.** (2007). Dissection of the autophagosome maturation
472 process by a novel reporter protein, tandem fluorescent-tagged LC3. *Autophagy* **3**, 452-60.
473 **Klionsky, D. J. Abdelmohsen, K. Abe, A. Abedin, M. J. Abeliovich, H. Acevedo Arozena,**
474 **A. Adachi, H. Adams, C. M. Adams, P. D. Adeli, K. et al.** (2016). Guidelines for the use and
475 interpretation of assays for monitoring autophagy (3rd edition). *Autophagy* **12**, 1-222.
476 **Kogure, T., Karasawa, S., Araki, T., Saito, K., Kinjo, M. and Miyawaki, A.** (2006). A
477 fluorescent variant of a protein from the stony coral Montipora facilitates dual-color single-laser
478 fluorescence cross-correlation spectroscopy. *Nat Biotechnol* **24**, 577-81.
479 **Kuma, A., Hatano, M., Matsui, M., Yamamoto, A., Nakaya, H., Yoshimori, T., Ohsumi, Y.,**
480 **Tokuhisa, T. and Mizushima, N.** (2004). The role of autophagy during the early neonatal
481 starvation period. *Nature* **432**, 1032-6.
482 **Kuma, A., Matsui, M. and Mizushima, N.** (2007). LC3, an autophagosome marker, can be
483 incorporated into protein aggregates independent of autophagy: caution in the interpretation
484 of LC3 localization. *Autophagy* **3**, 323-8.
485 **Lee, E., Koo, Y., Ng, A., Wei, Y., Luby-Phelps, K., Juraszek, A., Xavier, R. J., Cleaver, O.,**
486 **Levine, B. and Amatruda, J. F.** (2014). Autophagy is essential for cardiac morphogenesis
487 during vertebrate development. *Autophagy* **10**, 572-87.
488 **Lee, M. J., Lee, J. H. and Rubinsztein, D. C.** (2013). Tau degradation: the ubiquitin-
489 proteasome system versus the autophagy-lysosome system. *Prog Neurobiol* **105**, 49-59.
490 **Li, L., Wang, Z. V., Hill, J. A. and Lin, F.** (2014). New autophagy reporter mice reveal
491 dynamics of proximal tubular autophagy. *J Am Soc Nephrol* **25**, 305-15.
492 **Lopez, A., Lee, S. E., Wojta, K., Ramos, E. M., Klein, E., Chen, J., Boxer, A. L., Gorno-**
493 **Tempini, M. L., Geschwind, D. H., Schlotawa, L. et al.** (2017). A152T tau allele causes
494 neurodegeneration that can be ameliorated in a zebrafish model by autophagy induction. *Brain*
495 **140**, 1128-1146.
496 **Maday, S. and Holzbaur, E. L.** (2014). Autophagosome biogenesis in primary neurons follows
497 an ordered and spatially regulated pathway. *Dev Cell* **30**, 71-85.

498 **Maday, S. and Holzbaur, E. L.** (2016). Compartment-Specific Regulation of Autophagy in

499 Primary Neurons. *J Neurosci* **36**, 5933-45.

500 **Mathai, B. J., Meijer, A. H. and Simonsen, A.** (2017). Studying Autophagy in Zebrafish. *Cells*

501 **6**.

502 **Melendez, A., Talloczy, Z., Seaman, M., Eskelinen, E. L., Hall, D. H. and Levine, B.** (2003).

503 Autophagy genes are essential for dauer development and life-span extension in C. elegans.

504 *Science* **301**, 1387-91.

505 **Mijaljica, D., Prescott, M. and Devenish, R. J.** (2011). Microautophagy in mammalian cells:

506 revisiting a 40-year-old conundrum. *Autophagy* **7**, 673-82.

507 **Mizushima, N.** (2009). Methods for monitoring autophagy using GFP-LC3 transgenic mice.

508 *Methods Enzymol* **452**, 13-23.

509 **Mizushima, N., Kuma, A., Kobayashi, Y., Yamamoto, A., Matsubae, M., Takao, T.,**

510 **Natsume, T., Ohsumi, Y. and Yoshimori, T.** (2003). Mouse Apg16L, a novel WD-repeat

511 protein, targets to the autophagic isolation membrane with the Apg12-Apg5 conjugate. *J Cell*

512 *Sci* **116**, 1679-88.

513 **Mizushima, N., Noda, T., Yoshimori, T., Tanaka, Y., Ishii, T., George, M. D., Klionsky, D.**

514 **J., Ohsumi, M. and Ohsumi, Y.** (1998). A protein conjugation system essential for autophagy.

515 *Nature* **395**, 395-8.

516 **Mizushima, N., Yamamoto, A., Hatano, M., Kobayashi, Y., Kabeya, Y., Suzuki, K.,**

517 **Tokuhisa, T., Ohsumi, Y. and Yoshimori, T.** (2001). Dissection of autophagosome formation

518 using Apg5-deficient mouse embryonic stem cells. *J Cell Biol* **152**, 657-68.

519 **Mizushima, N., Yamamoto, A., Matsui, M., Yoshimori, T. and Ohsumi, Y.** (2004). In vivo

520 analysis of autophagy in response to nutrient starvation using transgenic mice expressing a

521 fluorescent autophagosome marker. *Mol Biol Cell* **15**, 1101-11.

522 **Mizushima, N., Yoshimori, T. and Levine, B.** (2010). Methods in mammalian autophagy

523 research. *Cell* **140**, 313-26.

524 **Mizushima, N., Yoshimori, T. and Ohsumi, Y.** (2011). The role of Atg proteins in

525 autophagosome formation. *Annu Rev Cell Dev Biol* **27**, 107-32.

Moreau, K., Fleming, A., Imarisio, S., Lopez Ramirez, A., Mercer, J. L., Jimenez-Sanchez, M., Bento, C. F., Puri, C., Zavodszky, E., Siddiqi, F. et al. (2014). PICALM modulates autophagy activity and tau accumulation. *Nat Commun* **5**, 4998.

Mostowy, S., Boucontet, L., Mazon Moya, M. J., Sirianni, A., Boudinot, P., Hollinshead, M., Cossart, P., Herbomel, P., Levraud, J. P. and Colucci-Guyon, E. (2013). The zebrafish as a new model for the in vivo study of Shigella flexneri interaction with phagocytes and bacterial autophagy. *PLoS Pathog* **9**, e1003588.

Ni, H. M., Bockus, A., Wozniak, A. L., Jones, K., Weinman, S., Yin, X. M. and Ding, W. X. (2011). Dissecting the dynamic turnover of GFP-LC3 in the autolysosome. *Autophagy* **7**, 188-204.

Otto, G. P., Wu, M. Y., Kazgan, N., Anderson, O. R. and Kessin, R. H. (2003). Macroautophagy is required for multicellular development of the social amoeba Dictyostelium discoideum. *J Biol Chem* **278**, 17636-45.

Panza, P., Maier, J., Schmees, C., Rothbauer, U. and Sollner, C. (2015). Live imaging of endogenous protein dynamics in zebrafish using chromobodies. *Development* **142**, 1879-84.

Pavel, M., Imarisio, S., Menzies, F. M., Jimenez-Sanchez, M., Siddiqi, F. H., Wu, X., Renna, M., O'Kane, C. J., Crowther, D. C. and Rubinsztein, D. C. (2016). CCT complex restricts neuropathogenic protein aggregation via autophagy. *Nat Commun* **7**, 13821.

Plucinska, G., Paquet, D., Hruscha, A., Godinho, L., Haass, C., Schmid, B. and Misgeld, T. (2012). In vivo imaging of disease-related mitochondrial dynamics in a vertebrate model system. *J Neurosci* **32**, 16203-12.

Renshaw, S. A. and Trede, N. S. (2012). A model 450 million years in the making: zebrafish and vertebrate immunity. *Dis Model Mech* **5**, 38-47.

Rosado, C. J., Mijaljica, D., Hatzinisiriou, I., Prescott, M. and Devenish, R. J. (2008). Rosella: a fluorescent pH-biosensor for reporting vacuolar turnover of cytosol and organelles in yeast. *Autophagy* **4**, 205-13.

Rubinsztein, D. C., Bento, C. F. and Deretic, V. (2015). Therapeutic targeting of autophagy in neurodegenerative and infectious diseases. *J Exp Med* **212**, 979-90.

554 **Rubinsztein, D. C., Cuervo, A. M., Ravikumar, B., Sarkar, S., Korolchuk, V., Kaushik, S.**

555 **and Klionsky, D. J.** (2009). In search of an "autophagomometer". *Autophagy* **5**, 585-9.

556 **Rusten, T. E., Lindmo, K., Juhasz, G., Sass, M., Seglen, P. O., Brech, A. and Stenmark,**

557 **H.** (2004). Programmed autophagy in the Drosophila fat body is induced by ecdysone through

558 regulation of the PI3K pathway. *Dev Cell* **7**, 179-92.

559 **Sanjuan, M. A., Milasta, S. and Green, D. R.** (2009). Toll-like receptor signaling in the

560 lysosomal pathways. *Immunol Rev* **227**, 203-20.

561 **Sargsyan, A., Cai, J., Fandino, L. B., Labasky, M. E., Forostyan, T., Colosimo, L. K.,**

562 **Thompson, S. J. and Graham, T. E.** (2015). Rapid parallel measurements of

563 macroautophagy and mitophagy in mammalian cells using a single fluorescent biosensor. *Sci*

564 *Rep* **5**, 12397.

565 **Sasaki, T., Lian, S., Khan, A., Llop, J. R., Samuelson, A. V., Chen, W., Klionsky, D. J. and**

566 **Kishi, S.** (2017). Autolysosome biogenesis and developmental senescence are regulated by

567 both Spns1 and v-ATPase. *Autophagy* **13**, 386-403.

568 **Sasaki, T., Lian, S., Qi, J., Bayliss, P. E., Carr, C. E., Johnson, J. L., Guha, S., Kobler, P.,**

569 **Catz, S. D., Gill, M. et al.** (2014). Aberrant autolysosomal regulation is linked to the induction

570 of embryonic senescence: differential roles of Beclin 1 and p53 in vertebrate Spns1 deficiency.

571 *PLoS Genet* **10**, e1004409.

572 **Schiebler, M., Brown, K., Hegyi, K., Newton, S. M., Renna, M., Hepburn, L., Klapholz, C.,**

573 **Coulter, S., Obregon-Henao, A., Henao Tamayo, M. et al.** (2015). Functional drug screening

574 reveals anticonvulsants as enhancers of mTOR-independent autophagic killing of

575 Mycobacterium tuberculosis through inositol depletion. *EMBO Mol Med* **7**, 127-39.

576 **Schmid-Burgk, J. L., Honing, K., Ebert, T. S. and Hornung, V.** (2016). CRISPaint allows

577 modular base-specific gene tagging using a ligase-4-dependent mechanism. *Nat Commun* **7**,

578 12338.

579 **Shaner, N. C., Campbell, R. E., Steinbach, P. A., Giepmans, B. N., Palmer, A. E. and**

580 **Tsien, R. Y.** (2004). Improved monomeric red, orange and yellow fluorescent proteins derived

581 from Discosoma sp. red fluorescent protein. *Nat Biotechnol* **22**, 1567-72.

582 **Shirakabe, A., Fritzky, L., Saito, T., Zhai, P., Miyamoto, S., Gustafsson, A. B., Kitsis, R.**
583 **N. and Sadoshima, J.** (2016). Evaluating mitochondrial autophagy in the mouse heart. *J Mol*
584 *Cell Cardiol* **92**, 134-9.

585 **Tanaka, Y., Watari, M., Saito, T., Morishita, Y. and Ishibashi, K.** (2016). Enhanced
586 Autophagy in Polycystic Kidneys of AQP11 Null Mice. *Int J Mol Sci* **17**.

587 **Tanida, I., Yamaji, T., Ueno, T., Ishiura, S., Kominami, E. and Hanada, K.** (2008).
588 Consideration about negative controls for LC3 and expression vectors for four colored
589 fluorescent protein-LC3 negative controls. *Autophagy* **4**, 131-4.

590 **Tian, F., Deguchi, K., Yamashita, T., Ohta, Y., Morimoto, N., Shang, J., Zhang, X., Liu, N.,**
591 **Ikeda, Y., Matsuura, T. et al.** (2010). In vivo imaging of autophagy in a mouse stroke model.
592 *Autophagy* **6**, 1107-14.

593 **Tian, F., Morimoto, N., Liu, W., Ohta, Y., Deguchi, K., Miyazaki, K. and Abe, K.** (2011). In
594 vivo optical imaging of motor neuron autophagy in a mouse model of amyotrophic lateral
595 sclerosis. *Autophagy* **7**, 985-92.

596 **Tsvetkov, A. S., Arrasate, M., Barmada, S., Ando, D. M., Sharma, P., Shaby, B. A. and**
597 **Finkbeiner, S.** (2013). Proteostasis of polyglutamine varies among neurons and predicts
598 neurodegeneration. *Nat Chem Biol* **9**, 586-92.

599 **Van Epps, H. A., Yim, C. M., Hurley, J. B. and Brockerhoff, S. E.** (2001). Investigations of
600 photoreceptor synaptic transmission and light adaptation in the zebrafish visual mutant nrc.
601 *Invest Ophthalmol Vis Sci* **42**, 868-74.

602 **Varga, M., Sass, M., Papp, D., Takacs-Vellai, K., Kobolak, J., Dinnyes, A., Klionsky, D. J.**
603 **and Vellai, T.** (2014). Autophagy is required for zebrafish caudal fin regeneration. *Cell Death*
604 *Differ* **21**, 547-56.

605 **Yoshimoto, K., Hanaoka, H., Sato, S., Kato, T., Tabata, S., Noda, T. and Ohsumi, Y.**
606 (2004). Processing of ATG8s, ubiquitin-like proteins, and their deconjugation by ATG4s are
607 essential for plant autophagy. *Plant Cell* **16**, 2967-83.

608 **Zhou, C., Zhong, W., Zhou, J., Sheng, F., Fang, Z., Wei, Y., Chen, Y., Deng, X., Xia, B.**
609 **and Lin, J.** (2012). Monitoring autophagic flux by an improved tandem fluorescent-tagged LC3

610   (mTagRFP-mWasabi-LC3) reveals that high-dose rapamycin impairs autophagic flux in

611   cancer cells. *Autophagy* **8**, 1215-26.

612

613

614

615   Figure Legends

616   Figure One: **Autophagosome formation**. (A) Schematic of autophagosome formation and

617   degradation: Within the cytoplasm, double-membraned, sac-like structures called a

618   phagophores are the first morphologically recognizable autophagic precursors and can be

619   distinguished within cells by the proteins that associate with their membranes. A complex

620   comprising ATG12–ATG5–ATG16L1 proteins enables the conjugation of LC3-II to the

621   membranes. The edges of the phagophore elongate and eventually fuse while engulfing a

622   portion of the cytoplasm. As the phagophore enlarges and approaches closure, the ATG5–

623   ATG12–ATG16L1 complex dissociates from the outer membrane, whereas LC3-II remains

624   associated. The resulting structure is a spherical double-membrane organelle, called the

625   autophagosome. Following closure, autophagosomes are trafficked by dynein motors along

626   microtubules to the perinuclear region where they fuse with the lysosomes and their contents

627   are degraded. (B) Lipidation of LC3-II: During autophagosome formation, LC3 (and other

628   ATG8 ubiquitin-like family proteins) are conjugated to the lipid phosphatidylethanolamine (PE)

629   in autophagosome membranes. This lipidation requires a protease and two ubiquitin-like

630   conjugation systems (explained in detail in Ichimura et al., 2000; Mizushima et al., 1998).

631   ATG4 is a cysteine protease which cleaves the C-terminus of LC3 exposing a glycine residue.

632   This first cleaved form of LC3 is called LC3-I. A further reaction then occurs involving a

633   complex of ATG12-5 and ATG16L1, which together act as an E3-like ligase. This determines

634   the site of LC3 lipidation and assists the transfer of LC3-I to PE in membranes to form LC3-II.

635   ATG8/LC3 proteins may assist in the expansion and closure of autophagosomal membranes,

636   in autophagosome-lysosome fusion and inner autophagosomal membrane degradation.

637

638   Figure Two: **Schematic diagram of conventional methods to measure rates of**

639   **autophagy.** (A&B) Western blots for LC3-II: Measuring LC3 lipidation by western blotting is

640   one of the best-established methods for measuring autophagic flux. However, care must be

641   taken in interpreting increases in LC3 levels as this may occur as a result of an increase in

642   autophagosome formation (upregulation) or a blockage in clearance. To discriminate between

643   these two scenarios, assays should be performed in basal conditions and in the presence of

644   an agent that prevents lysosomal degradation such as bafilomycin A1 (Baf) or ammonium

645   chloride (NH_4Cl). (A) When autophagy is induced, LC3-II levels increase as more

646   autophagosomes are formed. In the presence of a lysosomal blocker, LC3-II levels increase

647   further because increased autophagosome formation still occurs, but autophagosomes cannot

648   be cleared and therefore build up within the cell. (B) In some conditions when autophagy is

649   blocked (for example, if fusion with the lysosome is prevented), LC3-II levels can also increase

650   since autophagosomes may form but are not degraded. In this scenario, when LC3-II levels

651   are measured in the presence of Baf or NH_4Cl, LC3-II levels are unchanged. The difference

652   in patterns between (A) and (B) can be used to discriminate between autophagy induction and

653   blockage. (C) When LC3-labelled vesicles (puncta) are measured within cells with a single

654   fluorophore (e.g. cells expressing GFP-tagged LC3 or immunofluorescence labelling of the

655   endogenous protein), an increase in puncta can be observed both in autophagy inducing and

656   autophagy blockage conditions. N.B. Commercially available antibodies with cross-reactivity

657   to zebrafish LC3 are widely available from suppliers such as from Novus Biologicals (used in

658   He et al., 2009; Moreau et al., 2014; Lopez et al., 2017) and Cell Signaling Technology (used

659   in Sasaki et al., 2014).

660

661   Figure Three: **Schematic diagram of the tandem mRFP-EGFP-LC3 expression to monitor**

662   **autophagic flux.** (A) Representation of the reporter construct mRFP-EGFP-LC3 and the

663   behaviour of its transcript upon different pH conditions. Under neutral pH conditions, both

664   EGFP and RFP fluorescence is observed. Under acidic pH conditions, EGFP fluorescence is

665   quenched and only red fluorescence is observed. (B) mRFP-EGFP-LC3 labelling during

666   autophagosome biogenesis, maturation and degradation. Unlipidated mRFP-EGFP-LC3

667   remains in the cytoplasm (light yellow) whereas lipidated mRFP-EGFP-LC3 is recruited to both

668   inner and outer membranes of phagophores and double membrane autophagosomes. During

669   these steps of autophagosome formation, the fluorescent signal of both fluorophores, mRFP

670   and EGFP, is visible and vesicles appear as yellow puncta. Autophagosomes eventually fuse

671   with lysosomes to form autolysosomes. Under these acidic conditions, the contents within the

672   inner membrane are eventually degraded. The green fluorescent signal from EGFP is

673   quenched in the acidic lysosomal conditions whereas the mRFP signal remains, resulting in

674   red autolysosomes. (C) Representative images of a cell expressing mRFP-EGFP-LC3 with

675   different levels of autophagy. The combination of green and red fluorescent signals from

676   unlipidated mRFP-EGFP-LC3 results in a yellow background in the cytoplasm of the cells. The

677   intensity of this yellow may change dependent upon changes in the autophagy flux. Under low

678   autophagy conditions, most of mRFP-EGFP-LC3 remains unlipidated resulting in a yellow

679   background and only a few yellow or red vesicles (autophagosomes and autolysosomes) are

680   seen. After autophagy induction, many new autophagosomes form and are labelled with

681   lipidated LC3. These rapidly fuse with lysosomes. This can be observed as an increase in the

682   number of total vesicles and the ratio of red:yellow vesicles as well as reduced yellow

683   background. When autophagic flux is blocked, autophagosome formation may still occur. In

684   this scenario, autophagosomes and autolysosomes accumulate but cannot be degraded and

685   can be observed as yellow puncta. The continuous lipidation of mRFP-EGFP-LC3 as new

686   autophagosomes form reduces the yellow background of the cytoplasm.

687   Figure Four: **Schematic diagram of the GFP-LC3-RFP-LC3DG reporter to measure**

688   **autophagic flux.** (A) Schematic diagram of the GFP-LC3-RFP-LC3DG reporter construct.

689   The GFP-LC3-RFP-LC3DG protein is cleaved by ATG4 resulting in the release of GFP-LC3

690   and RFP-LC3DG in equimolar amounts. (B) GFP-LC3 becomes lipidated and binds to

691   autophagosomes and autophagosome precursors and can be visualised as green vesicles

692   (puncta), whereas unlipidated RFP-LC3DG remains in the cytoplasm. The GFP signal is

693   quenched when autophagosomes fuse to lysosomes to form autolysosomes. The green signal

694   can therefore be used as a marker for phagophores and autophagosomes, but autolysosomes

695   are not labelled. (C) Representative images of a cell expressing GFP-LC3-RFP-LC3DG with

696   different levels of autophagy. The unlipidated RFP-LC3DG is released as an internal control

697   at the same rate and amount as GFP-LC3 and always remains cytosolic. Levels of red signal

698   are independent of autophagy degradation and remain unchanged upon autophagy

699   perturbation. GFP-LC3 however can be found unlipidated free in the cytoplasm or lipidated

700   hence bound to autophagic membranes and therefore susceptible to autophagy degradation.

701   Under high levels of autophagic flux, GFP-LC3 becomes lipidated and degraded, and thereby

702   the level of green signal is reduced. When autophagy is blocked, the accumulation of

703   unlipidated GFP-LC3 and the lack of degradation of the lipidated form results in an increase

704   in the GFP signal. The ratio of the GFP:RFP (i.e. the green signal from GFP-LC3 and the

705   unchanged mRFP-LC3DG) is then used to measure the rate of autophagic flux.

706

707   Figure Five: **Measuring autophagy substrate clearance *in vivo*.** (A) Zebrafish were

708   generated which express the fluorescent, photoconvertible protein Dendra tagged to human

709   tau, a known autophagy substrate. The green fluorescent Dendra protein can be

710   photoconverted to a red fluorescent protein by exposure to 405 nm light. (B) Mosaic

711   expression of the transgene allows individual neurons in the spinal cord to be identified and

712   selected for photoconversion. Images of the same neurons were taken before and

713   immediately after photoconversion and then at 12-hour intervals. The amount of red

714   fluorescent signal was quantified at each time point and used to calculate the clearance of tau

715   protein. (C) Schematic diagram of the clearance kinetics of tau following in response to

716   manipulation of autophagic flux. Treatment with autophagy inducers (green) accelerates the

717   clearance of tau protein whereas treatment with autophagy blockers (red) slows the clearance

718   kinetics.

719

720

721   Table One: Comparison of zebrafish and human orthologues of ATG8

Zebrafish gene	Description	Ensembl ID	Human orthologue	Percentage identity to human orthologue
Map1lc3a	microtubule-associated protein 1 light chain 3 alpha	ENSDARG00000033609	MAP1LC3A	85.95%
Map1lc3b	microtubule-associated protein 1 light chain 3 beta	ENSDARG00000101127	MAP1LC3B2	92.62%
Map1lc3c	microtubule-associated protein 1 light chain 3 gamma	ENSDARG00000100528	MAP1LC3C	65.47%
Map1lc3cl	microtubule-associated protein 1 light chain 3 gamma, like	ENSDARG00000075727	No human orthologue	(58.73% identity to zebrafish map1lc3c)
gabarapa	GABA(A) receptor-associated protein a	ENSDARG00000035557	GABARAP	93.44%
gabarapb	GABA(A) receptor-associated protein b	ENSDARG00000052082	GABARAP	75.66%
Unnamed	Unnamed	ENSDARG00000040971	GABARAPL1	58.97%
gabarapl2	GABA(A) receptor-associated protein like 2	ENSDARG00000027200	GABARAPL2	96.58%

722

723

A.

Lysosome

Pre-autophagosomal structures   Autophagosome   Autolysosome

Atg5, Atg12, Atg16l
LC3-II

Autophagic cargo

B.

LC3 → (Atg4) → LC3-I—Gly → (Atg7) (Atg3) → LC3-II →

PE

LC3-II   LC3-II   LC3-II

A. Inducer

LC3- II

LC3/actin ratio
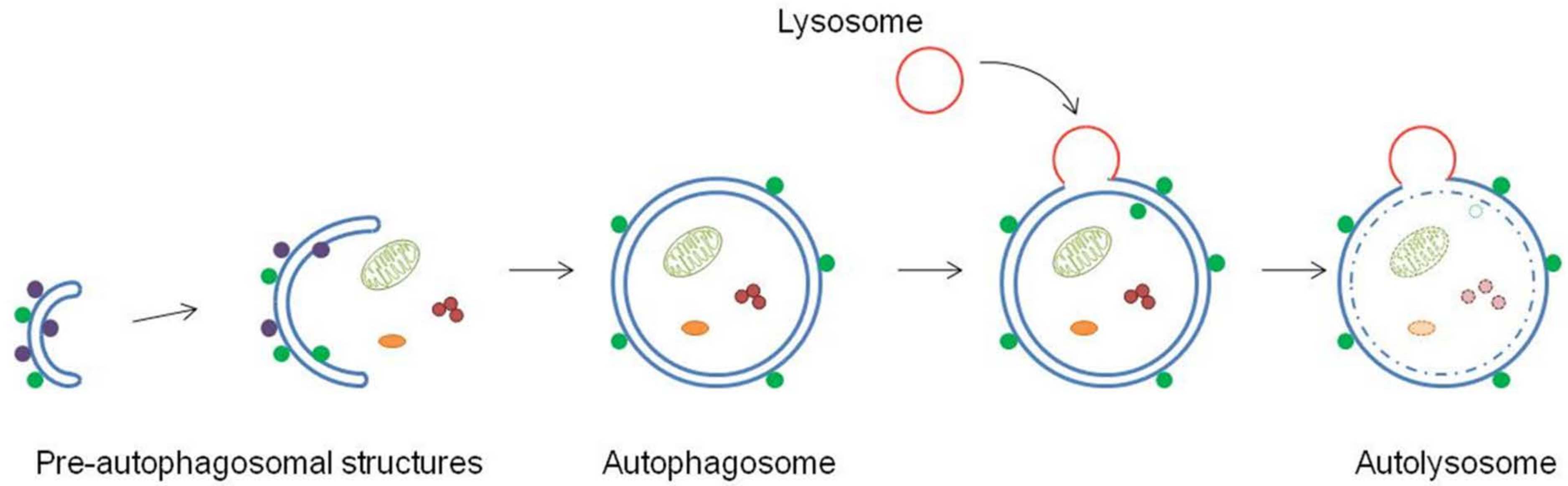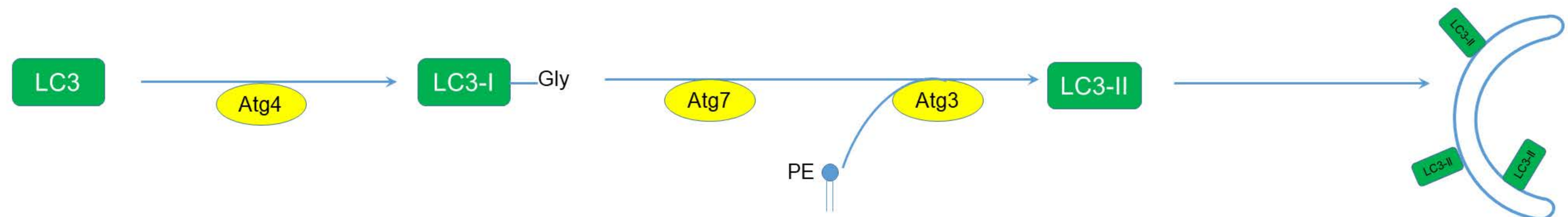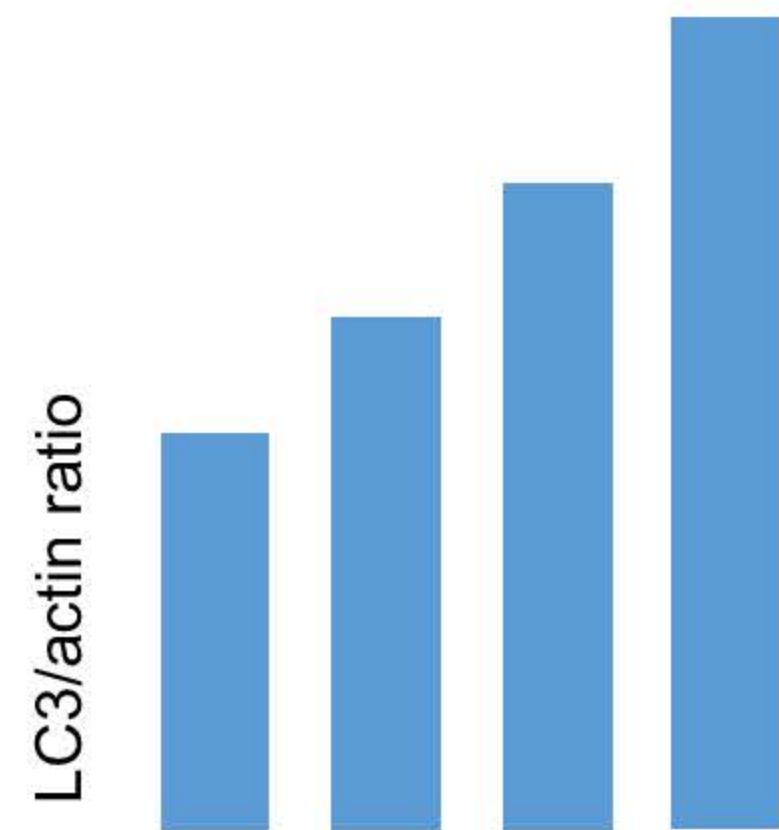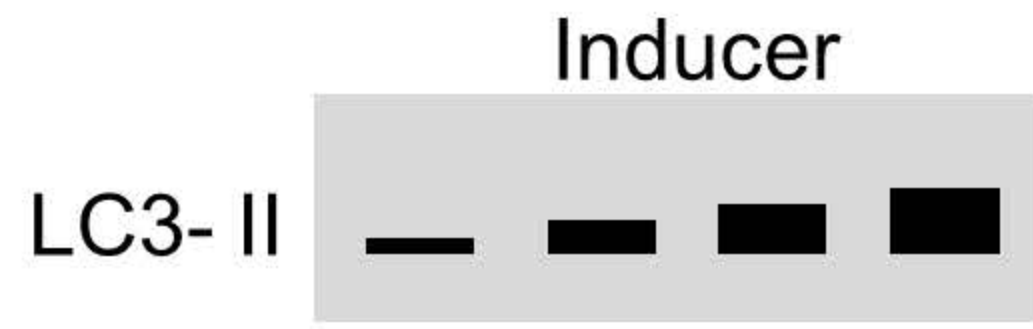
| Autophagy Inducer | − | + | − | + |
| Baf/NH$_4$Cl | − | − | + | + |

B. Blocker

LC3- II

LC3/actin ratio
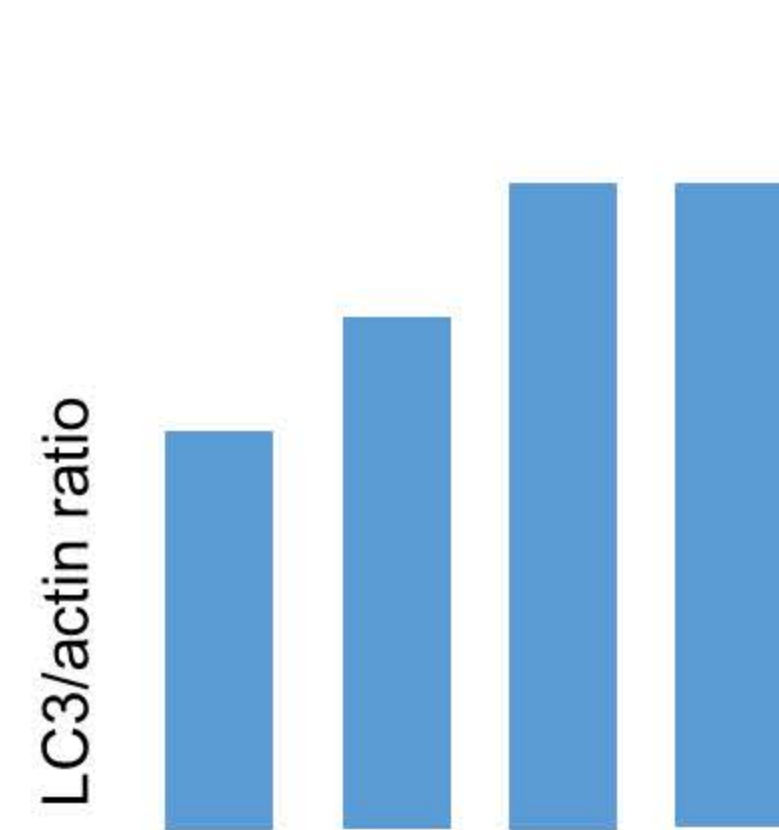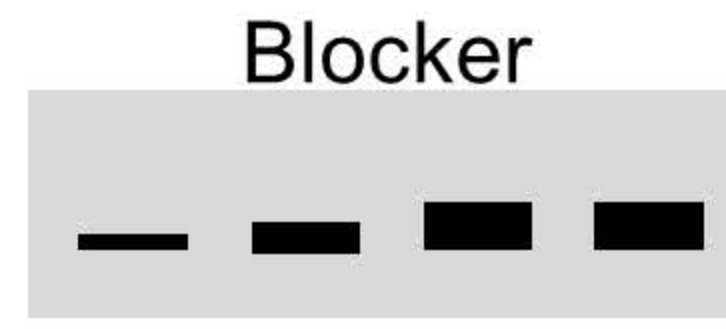
| Autophagy Blocker | − | + | − | + |
| Baf/NH$_4$Cl | − | − | + | + |

C.

Basal autophagy
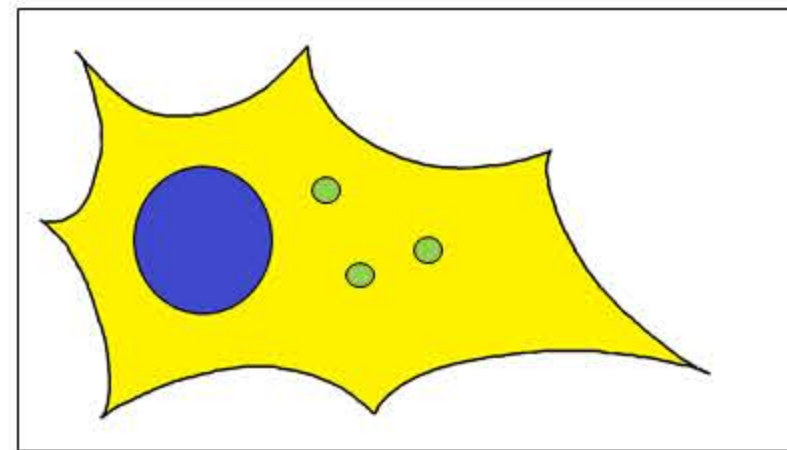
Autophagy inducer
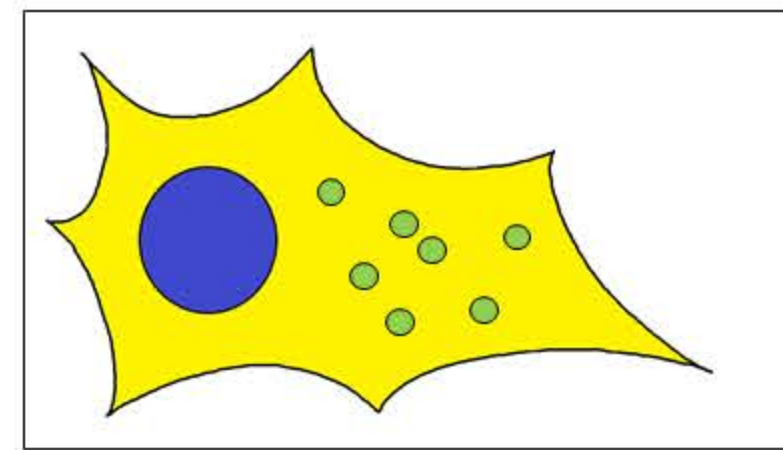
Autophagy blocker
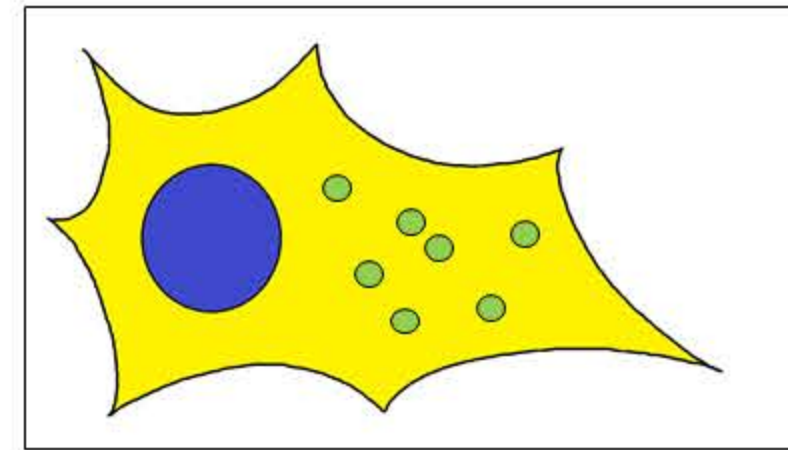
○ LC3-positive vesicle

Figure Two

A.

Promoter | mRFP | EGFP | LC3

Neutral pH

mRFP | EGFP | LC3

Acidic pH

mRFP | EGFP | LC3

B.

Phagophore

Lysosome

Nucleus
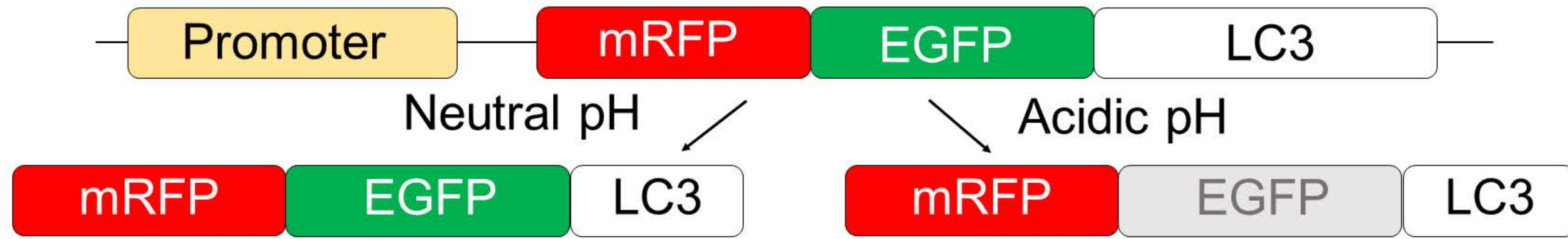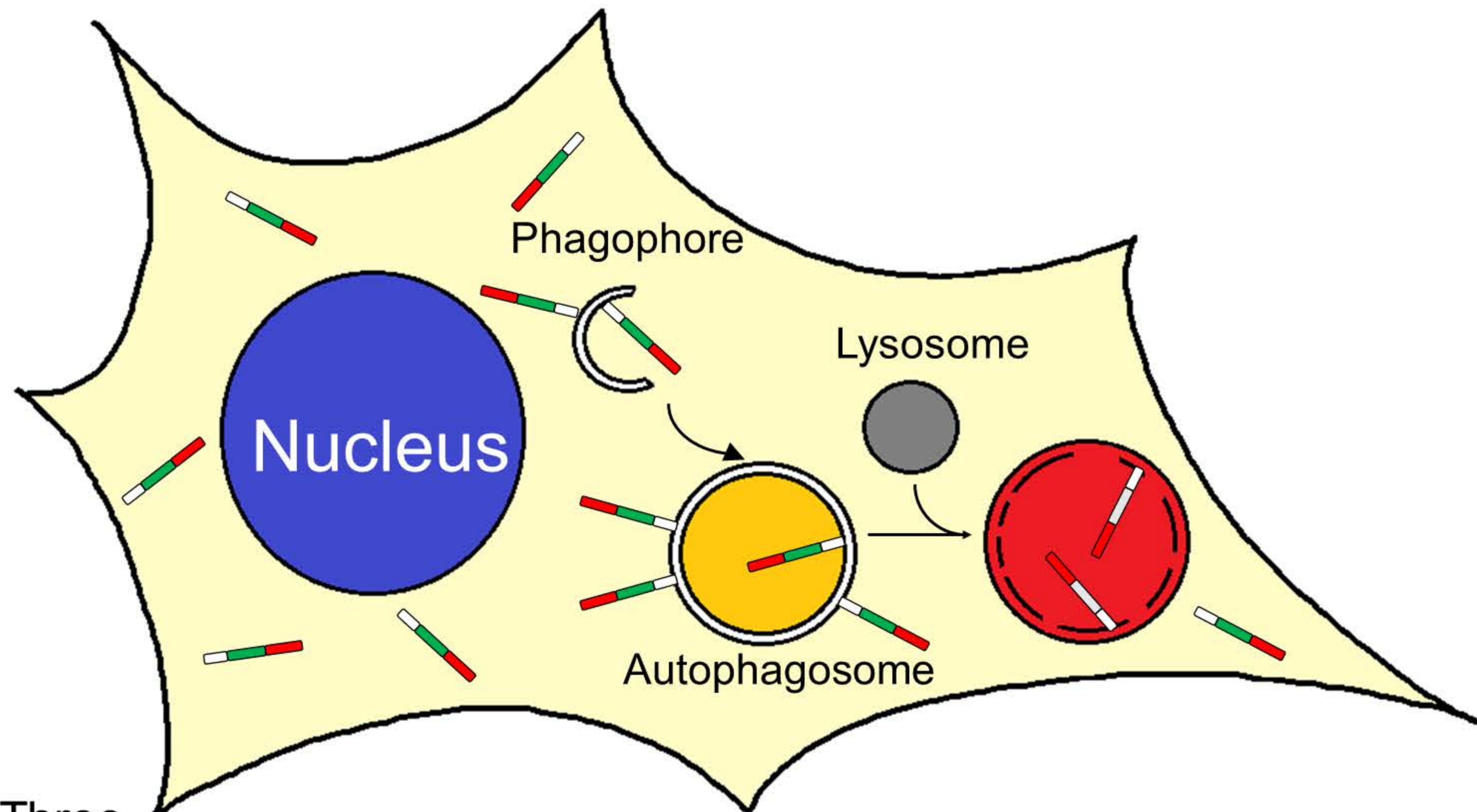
Autophagosome

C.
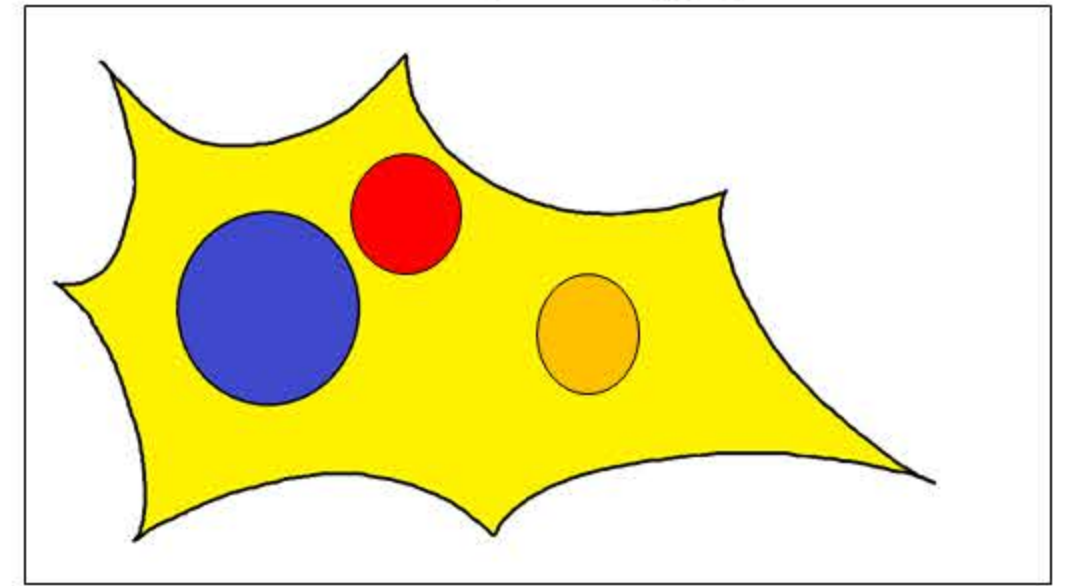
Low autophagy

High autophagy
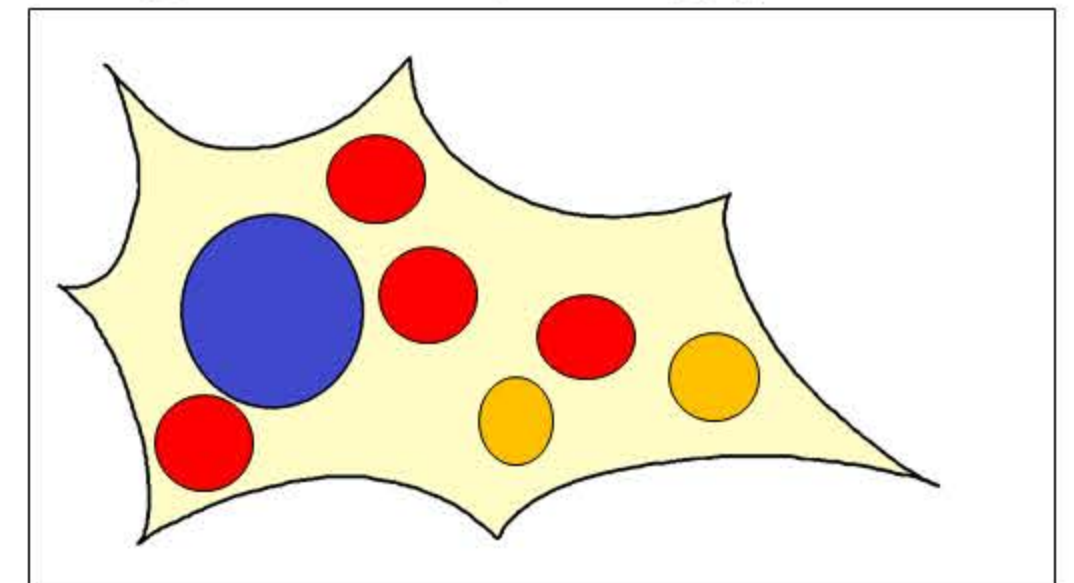
Autophagy blockade

● Autophagosome
● Autolysosome

Figure Three

A.

EF1a — GFP — LC3 — RFP — LC3ΔG

Atg4

GFP — LC3
Autophagy substrate

RFP — LC3ΔG
Internal control

B.

Phagophore
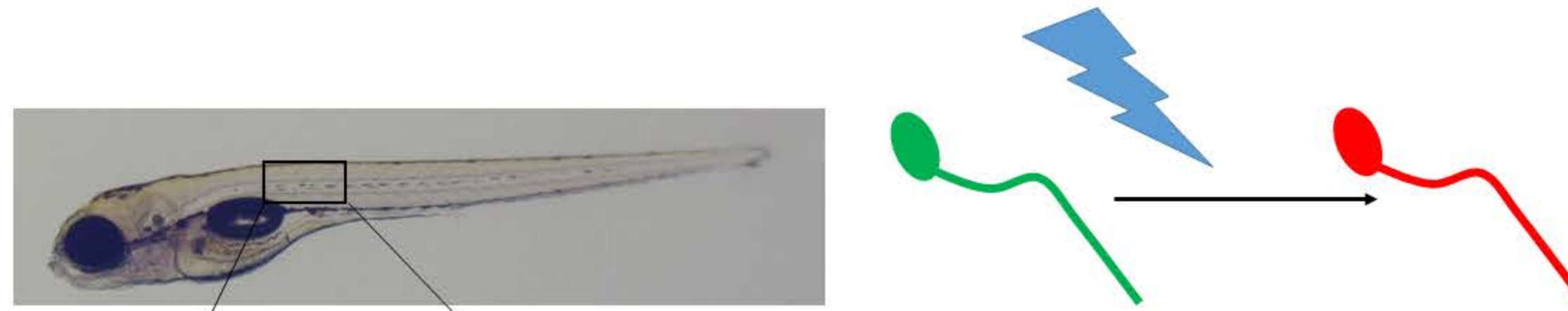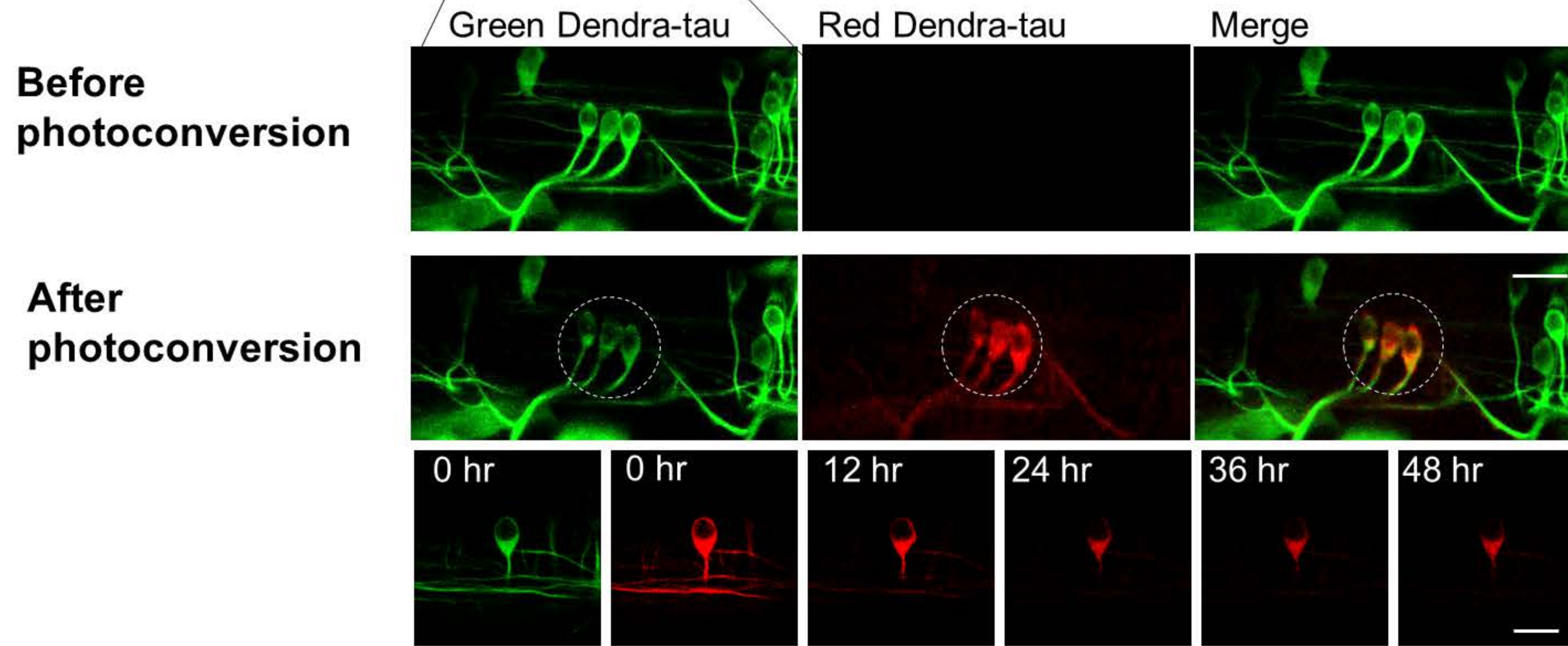
Lysosome

Nucleus

Autophagosome

C.

RFP

GFP

Merge

High   Low

Autophagy flux

Figure Four

A.

B.

	Green Dendra-tau	Red Dendra-tau	Merge
Before photoconversion			
After photoconversion			

0 hr   0 hr   12 hr   24 hr   36 hr   48 hr

C.

% Dendra-tau

Time

— Autophagy blocker
— Basal clearance rate
— Autophagy inducer

Figure Five